

Active nematic response to a deformable body or boundary: elastic deformations and anchoring-induced flow

Thomas G. J. Chandler^{1,*} and Saverio E. Spagnolie^{1,†}

¹*Department of Mathematics, University of Wisconsin–Madison, Madison, WI 53706, USA*

(Dated: September 25, 2024)

A body immersed in a nematic liquid crystal disturbs the fluid’s preferred molecular configuration and increases its stored elastic energy. In an active nematic, the fluid components also generate a stress in the bulk fluid. By introducing either an immersed body or boundary, a fluid flow can be triggered due to anchoring boundary conditions. The fluid imposes elastic, viscous, and active stresses on such surfaces, which, if compliant, may result in a surface deformation. We study the deformations and stress in a linearly elastic body placed in an active nematic in two-dimensions. Using complex variables techniques, exact expressions for the fluid flow, director field, surface tractions, and body deformation are derived. Qualitative differences between elastic and active stress-driven deformations are identified, depending on an active Ericksen number, anchoring conditions, and body material properties, thereby suggesting a new method for measuring the active stresses in active anisotropic biological systems. Flow profiles, external confinement, and anchoring-induced stirring are also addressed.

The eukaryotic cell is host to a wide variety of deformable organelles, from the nucleus to mitochondria [1–6]. These organelles exist in a complex, potentially anisotropic, viscous environment [7, 8], and experience mechanical stresses due to actively driven cytoplasmic flows [9]. The cell membrane itself is also deformable, and is commonly remodelled by internal processes. For instance, active anisotropic stresses are of great functional importance in cytoskeletal remodeling of the nucleus and chromatin configurations [10, 11], and in the metaphase spindle [12–14]. On a larger length scale, active systems like bacterial swarms and biofilms also exhibit anisotropy, among other complex rheological properties [15–18]. Understanding how such bodies affect, and are affected by, this complex environment is of generic importance.

Even when free of bodies, actively-driven anisotropic flows exhibit very rich and complex dynamics [19–23]. Stability [21, 24–30], topology [31], pattern formation [32–34], and mixing [35, 36] have seen substantial theoretical treatment. Confinement introduces an additional length scale, which can affect the emergent spatial structure [37, 38]. Strong active nematic stresses can also change the shape of deformable confining surfaces [39–46], and they play a prominent role in directing the motility of cells [47, 48] and active droplets [49–52].

When an active nematic contains an immersed body, or inclusion, additional elastic stresses are immediately introduced. In passive systems, these stresses result in intricate and beautiful textures [53–55], and can be used to measure cell material properties [56, 57]. In the presence of activity, the combination of fluid elasticity and anisotropy redirects actively driven flows, leading to complex immersed body dynamics. Recent examples include an investigation of the biased rotation of gear-like bodies [58, 59], and transitions from fixed point to limit cycle to chaotic dynamics of a circular disk [60]. How body deformability affects, and is affected, by such an active

environment has not been well explored.

In this letter, we present a model for an active anisotropic fluid with a soft internal or external boundary, confined to two-dimensions (2D). The model integrates Ericksen–Leslie theory [61–63] for active nematic liquid crystals (LCs), a common model for active anisotropic fluid [23, 64], and linear elasticity for deformable solids. Complex variable techniques yield novel analytical representations for the director field, velocity field, and boundary deformation. We demonstrate this for both an immersed and bounding cylinder, highlighting the insights that these analytical solutions provide.

Active nematic LCs can be described by their locally-averaged molecular orientation, $\mathbf{n}(\mathbf{x}, t)$, and fluid velocity $\mathbf{u}(\mathbf{x}, t)$, with spatial position \mathbf{x} , time t , and $|\mathbf{n}| = 1$. The director field, \mathbf{n} , evolves due to gradients in the velocity field, with strain rate tensor $\mathbf{E} = (\nabla\mathbf{u} + \nabla\mathbf{u}^T)/2$ and vorticity tensor $\mathbf{\Omega} = (\nabla\mathbf{u} - \nabla\mathbf{u}^T)/2$, and a relaxation towards equilibrium under the action of the molecular field, \mathbf{h} . In the one-constant approximation, $\mathbf{h} = K\nabla^2\mathbf{n}$, for the single (Frank) elastic constant K . Altogether,

$$\partial_t\mathbf{n} + \mathbf{u} \cdot \nabla\mathbf{n} = \mathbf{n} \cdot \mathbf{\Omega} + \lambda\mathbf{n} \cdot \mathbf{E} \cdot (\mathbf{I} - \mathbf{nn}) + \tilde{\mathbf{h}}/\gamma, \quad (1)$$

with γ rotational viscosity, λ tumbling/reactive parameter, and $\tilde{\mathbf{h}} = (\mathbf{I} - \mathbf{nn}) \cdot \mathbf{h}$ the transverse part of the molecular field, where \mathbf{nn} is a dyadic product [61–63]. Assuming incompressibility, the fluid velocity satisfies the momentum and mass conservation equations

$$\nabla \cdot (\boldsymbol{\sigma}^e + \boldsymbol{\sigma}^v + \boldsymbol{\sigma}^a - p\mathbf{I}) = \mathbf{0} \quad \text{and} \quad \nabla \cdot \mathbf{u} = 0, \quad (2a,b)$$

for the pressure p and elastic, viscous, and active stress tensors

$$\boldsymbol{\sigma}^e = -K\nabla\mathbf{n} \cdot \nabla\mathbf{n}^T + \frac{1}{2}(1 - \lambda)\mathbf{n}\tilde{\mathbf{h}} - \frac{1}{2}(1 + \lambda)\tilde{\mathbf{h}}\mathbf{n}, \quad (3a)$$

$$\boldsymbol{\sigma}^v = 2\mu\mathbf{E} + \mu_1(\mathbf{n} \cdot \mathbf{E} \cdot \mathbf{n})\mathbf{nn} + \mu_2(\mathbf{n}\mathbf{E} \cdot \mathbf{n} + \mathbf{n} \cdot \mathbf{E}\mathbf{n}), \quad (3b)$$

$$\boldsymbol{\sigma}^a = 2\alpha\mathbf{nn}, \quad (3c)$$

respectively. Here, μ is the solvent viscosity, μ_1 and μ_2 are anisotropic viscosities, and α is the activity strength, which can describe both extensile ($\alpha < 0$) and contractile ($\alpha > 0$) activity [23, 64, 65].

We non-dimensionalize the system by using an intrinsic length scale L (*e.g.* the size of an immersed body), velocity scale U (to be defined), and stress scale K/L^2 . The dimensionless system is then described by the dimensionless Ericksen number, activity strength, and viscosity ratios [66]:

$$\text{Er} := \frac{\mu UL}{K}, \quad A := \frac{\alpha L}{\mu U}, \quad \gamma' := \frac{\gamma}{\mu}, \quad \mu'_j := \frac{\mu_j}{\mu}. \quad (4a-d)$$

For small rotational Ericksen numbers, $\gamma' \text{Er} \ll 1$, the fluid flow does not affect the director field and the molecular field relaxes to equilibrium. The director evolution equation (1) takes the dimensionless form

$$\tilde{\mathbf{h}} = (\mathbf{I} - \mathbf{nn}) \cdot \nabla^2 \mathbf{n} = \mathcal{O}(\gamma' \text{Er}). \quad (5)$$

By further assuming small viscosity ratios, $\gamma', \mu'_i \ll 1$, the momentum equation (2a) takes the dimensionless form

$$\nabla^2 \mathbf{u} - \nabla p = \frac{1}{\text{Er}} \nabla \cdot (\nabla \mathbf{n} \cdot \nabla \mathbf{n}^T) - 2A \nabla \cdot (\mathbf{nn}), \quad (6)$$

up to $\mathcal{O}(\gamma', \mu'_i)$. This describes an isotropic Stokes flow with active and elastic driving forces [66].

In the examples presented in this letter, the fluid flow is induced by activity alone; thus, the velocity scale is set by the activity strength, $U = |\alpha|L/\mu$, and the assumption of a small Ericksen number is equivalent to assuming weak activity, $\gamma' \text{Er} = |\alpha|\gamma L^2/(\mu K) \ll 1$. Furthermore, in 2D, the assumption of a small viscosity ratio μ'_2 is unnecessary since it only corresponds to an anisotropy out-of-the-plane. Instead, μ_2 can be absorbed into the isotropic viscosity by taking $\mu \mapsto \mu - \mu_2/2$.

In two dimensions, the director field can be described by a director angle $\theta(x, y) \in [0, \pi)$ such that $\mathbf{n} = (\cos \theta, \sin \theta)$. Additionally, the conservation of mass (2b) implies that a streamfunction $\psi(x, y)$ can be introduced such that $\mathbf{u} = (\partial_y \psi, -\partial_x \psi)$. In this case, the equilibrium equation (5) reduces to Laplace's equation, $\nabla^2 \theta = 0$, while the momentum equation (6) is equivalent to a Poisson's equation for the scalar vorticity, $\omega = -\nabla^2 \psi$. Here, we absorb the isotropic parts of the stress tensors into the pressure by taking $p \mapsto p + A - |\nabla \theta|^2/(2\text{Er})$.

At any boundaries, the fluid velocity is assumed to vanish, while the director relaxes to some preferential angle ϕ with some anchoring strength W (*i.e.* Rapini-Papoular anchoring [67]):

$$\partial_x \psi = \partial_y \psi = 0 \quad \text{and} \quad \partial_\nu \theta = (w/2) \sin[2(\theta - \phi)], \quad (7a,b)$$

for the normal derivative pointing into the LC $\partial_\nu = \hat{\nu} \cdot \nabla$ and the dimensionless anchoring strength $w := WL/K$.

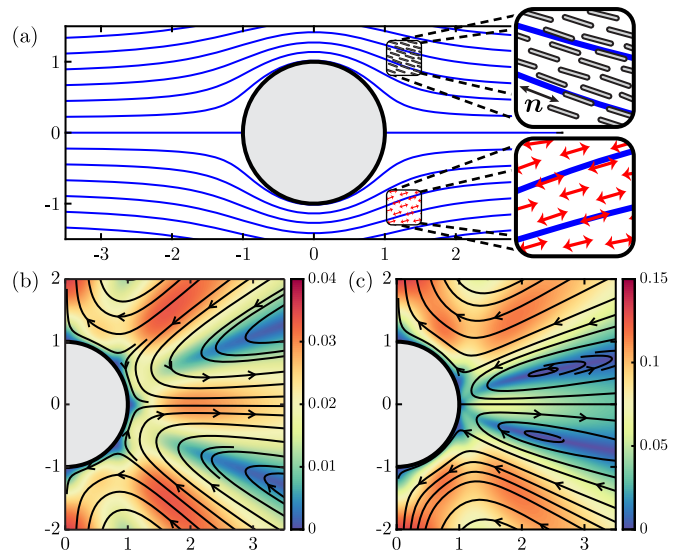


FIG. 1. The activity-induced flow of a 2D nematic LC outside a cylinder for $A = -1$ (*i.e.* extensile activity). (a) The director lines for $w = 10$ are shown as blue curves. (b,c) The activity-induced velocity field is shown for (b) $w = 1$ and (c) $w = 10$. The black arrows show the flow direction and the color denotes the fluid speed, $\sqrt{u^2 + v^2}$. Contractile activity with $A = 1$ corresponds to flipping the flow direction.

Consider the complex position $z = x + iy$ and its complex conjugate $\bar{z} = x - iy$. Using the Wirtinger derivatives, $\partial_x = \partial_z + \partial_{\bar{z}}$ and $\partial_y = i\partial_z - i\partial_{\bar{z}}$, one can make a change of variables from (x, y) to (z, \bar{z}) [68]. In these complex coordinates, the system takes the form

$$\partial_{z\bar{z}} \theta = 0 \quad \text{and} \quad \partial_{\bar{z}}(p - i\omega) = A \partial_z e^{2i\theta}, \quad (8a,b)$$

with vorticity $\omega = -4\partial_{z\bar{z}} \psi$ and velocity, $\mathbf{u} = (u, v)$, given by $u - iv = 2i\partial_z \psi$. Integrating (8) yields

$$\theta = -\arg f'(z) \quad (9a)$$

$$\text{and} \quad p - i\omega = A \partial_z [g(z) + \overline{f(z)}/f'(z)], \quad (9b)$$

for some locally-holomorphic functions f and g [68]. (Throughout, we shall assume the LC does not contain any topological defects, and so, f is non-zero and singularity free inside the LC.) Inserting the imaginary part of (9b) into $\partial_{z\bar{z}} \psi = -\omega/4$ and integrating yields

$$\psi = \frac{A}{4} \text{Im} \left[\bar{z}g(z) + h(z) + \int f(z) dz / f'(z) \right], \quad (10)$$

for another locally-holomorphic function h . The first two terms in (10) correspond to the well-known form of a biharmonic function with Goursat functions h and g [69]. The last term is a particular solution that accounts for the active forcing.

Analytical solutions for the director and velocity fields are thus obtained, provided that functions f , g , and h , which are locally holomorphic within the LC and satisfy the boundary conditions in (7), may be found. The

problem for f derived here is equivalent to the potential problem explored in Refs. [70, 71] for a passive LC. It is important to note that the solutions (9)–(10) are not invariant under a conformal mapping since they contain a mixture of holomorphic (function of z) and antiholomorphic (function of \bar{z}) terms.

As an example, consider a cylinder of radius L of infinite extent immersed in a weakly-active nematic LC. In the far-field, we assume the LC is aligned horizontally in a direction orthogonal to the cylinder's long axis and the fluid velocity vanishes. Additionally, the LC is assumed to be tangentially anchored to the cylinder with a finite strength, *i.e.* (7b) with $\phi = \arg(iz) \bmod \pi$ on $|z| = 1$. Without the body, the system sits at an equilibrium, with $\mathbf{n} = \hat{\mathbf{x}}$ and $\mathbf{u} = \mathbf{0}$, and the active stress is absorbed by the pressure.

First, we determine the LC director angle $\theta = -\arg f'$. Here, the potential $f(z)$ must be locally holomorphic in $1 < |z| < \infty$ and satisfy the finite anchoring condition on $|z| = 1$, and $f(z) \sim z$ as $|z| \rightarrow \infty$. The solution to this problem that minimizes the Frank elastic energy is, for any $w > 0$,

$$\theta = -\arg f'(z) = -\arg(1 - \rho^2/z^2), \quad (11)$$

where $\rho(w) := (\sqrt{1 + 4/w^2} - 2/w)^{1/2}$ is an effective radius [70]. The corresponding director lines (which lay parallel to \mathbf{n}) are plotted in Fig. 1(a) for $w = 10$.

Next, with (11), we determine the activity-induced fluid flow. Here, the Goursat functions $h(z)$ and $g(z)$ must be locally holomorphic in $1 < |z| < \infty$ and yield a fluid velocity that vanishes on $|z| = 1$ and as $|z| \rightarrow \infty$, ultimately yielding the streamfunction

$$\psi = \frac{A\rho^2}{8} \operatorname{Im} \left[\frac{(|z|^2 - 1)^2}{z^2(z^2 - \rho^2)} + \frac{1 - |z|^2 + 2 \log |z|}{(z^2 - \rho^2)/(2\rho^2)} \right], \quad (12)$$

see [66]. The corresponding velocity field is shown in Fig. 1(b,c) for $w = 1$ and $w = 10$, with $A = -1$ (*i.e.* extensile activity). A prominent feature is a plume extending symmetrically to both the left and right of the cylinder. Far from the body, the velocity field behaves as

$$u + iv \sim [\rho^2 \cos(2\alpha) - \cos(4\alpha)] A \rho^2 e^{i\alpha} / (2|z|), \quad (13)$$

as $|z| \rightarrow \infty$, for $\alpha = \arg z$; the plume angle thus decreases from $\pi/4$ to 0 as the anchoring strength w is increased from 0 to ∞ , while the plume speed is largest at $w = 8/3$. The velocity field does not appear as a dipole or stresslet in the far-field — the mere presence of the body initiates additional flow far away due to the distributed active stress, leading to bulk flow release. This also demonstrates that a body with non-trivial anchoring conditions is sufficient to induce a large scale flow through its presence alone.

Both the elasticity associated with passive LCs and the flow induced by activity generate stresses that act

on any boundaries. Here, the passive LC introduces a surface traction $\mathbf{t}^e = \hat{\boldsymbol{\nu}} \cdot \hat{\boldsymbol{\sigma}}^e + \partial_s \mathbf{t}^s$, where $\hat{\boldsymbol{\sigma}}^e = (1/2)|\nabla\theta|^2 \mathbf{I} - \nabla\theta\nabla\theta$ is the (traceless) elastic stress tensor and \mathbf{t}^s is a surface stress vector caused by the finite surface-anchoring (7b) [66]. The activity generates an additional surface traction $\mathbf{t}^a = \operatorname{Er} \hat{\boldsymbol{\nu}} \cdot (\hat{\boldsymbol{\sigma}}^v + A\hat{\boldsymbol{\sigma}}^a - p\mathbf{I})$ for the (traceless) viscous and active stress tensors $\hat{\boldsymbol{\sigma}}^v = \nabla\mathbf{u} + \nabla\mathbf{u}^T$ and $\hat{\boldsymbol{\sigma}}^a = 2\mathbf{n}\mathbf{n} - \mathbf{I}$, respectively.

If a boundary is soft, it will generally be deformed by the surface tractions above. We assume the boundary is part of an isotropic solid that deforms according to plane stress/strain in the framework of linear elasticity, with shear modulus μ_s and Poisson's ratio ν [72, 73]. In this framework, the deformed (Eulerian) frame and the reference (Lagrangian) frame are mathematically equivalent. At equilibrium, the elastic solid can be described by an Airy-stress function, $\mathcal{A}(x, y)$, which satisfies the biharmonic equation, $\nabla^4 \mathcal{A} = 0$. We can, thus, write

$$\mathcal{A} = \operatorname{Im}[\bar{z}G(z) + H(z)], \quad (14)$$

for two (new) Goursat functions, G and H , that are locally holomorphic within the solid (but not necessarily the LC), analogous to g and h in (10) [72]. These Goursat functions yield the stress tensor within the solid, $\boldsymbol{\Sigma}$, via the Kolosov–Muskhelishvili formulae [66]. Additionally, the solid displacement, (U, V) , can be expressed as

$$2M(U - iV) = i\kappa\overline{G(z)} + i\bar{z}G'(z) + iH'(z), \quad (15)$$

up to an arbitrary body displacement and rotation, for the dimensionless elastic modulus $M := \mu_s L^2 / K$ and $\kappa = (3 - 4\nu)$ or $(3 - \nu)/(1 + \nu)$ for plane strain or plane stress, respectively.

The LC–solid interface must also be at equilibrium, and so, the stresses acting on it must balance: $-\hat{\boldsymbol{\nu}} \cdot \boldsymbol{\Sigma} = \mathbf{t}^e + \mathbf{t}^a$. Provided we can find functions G and H that are locally holomorphic within the solid and satisfy this stress balance, we will have obtained analytic solutions for the solid's deformation. However, yet again, the above solution is not invariant under a conformal map, and analytical progress can only be made in specific cases.

We return to the example of a unit cylinder subject to (finite) tangential anchoring. Here, the director angle (11) and streamfunction (12) yield analytic expressions for the elastic traction, $t_x^e + it_y^e$, and activity-induced traction, $t_x^a + it_y^a = A \operatorname{Er}(1/z - \rho^2 z)$, acting on the cylinder. The cylinder is now assumed to be deformable, and so, we seek the Airy stress (14). The Goursat functions $G(z)$ and $H(z)$ must be locally holomorphic in $|z| < 1$ and satisfy the stress balance condition on $|z| = 1$. See [66] for the solution to this problem.

For passive LCs ($A = 0$), the deformation acts to reduce the elastic energy stored in the LC by flattening the cylinder. Figure 2 shows the LC configurations and body deformations for three different anchoring strengths and $\kappa = 5/3$ (*i.e.* an incompressible cylinder, $\nu = 1/2$, under

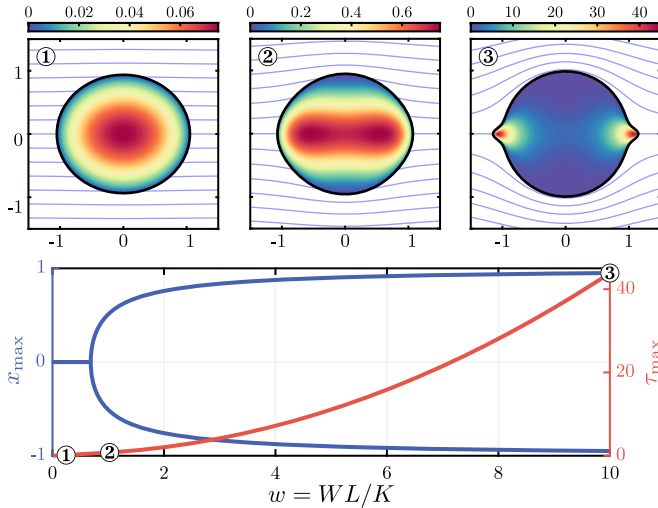


FIG. 2. (top) Deformation of soft cylinders immersed in passive nematic LCs with $A\text{Er} = 0$, $M/w = 5$, $\kappa = 5/3$, and dimensionless anchoring strengths ① $w = 0.1$, ② $w = 1$, and ③ $w = 10$. Color indicates the maximum shear stress, $\tau = \sqrt{(\Sigma_{xx} - \Sigma_{yy})^2/4 + \Sigma_{xy}^2}$, within the cylinder and the blue curves are director lines. (bottom) The positions, $(x_{\max}, 0)$, and value, τ_{\max} , of the largest maximum shear stress plotted as a function of w .

plane stress). For large anchoring strengths, $w \gg 1$, most of the LC energy is stored local to the left and right poles of the cylinder, with a singular energy emerging in the case of strong (infinite) anchoring ($w = \infty$) due to the appearance of two -1 Boojum topological defects at $z = \pm 1$ [70, 74]. This localization of energy within the LC results in large localized surface tractions: $t_x^e + it_y^e = \mathcal{O}(w^2)$ for $z \pm 1 = \mathcal{O}(1/w)$, and $t_x^e + it_y^e = \mathcal{O}(1)$ otherwise, as $w \rightarrow \infty$. This, in turn, leads to large localized deformations of the cylinder, see Fig. 2. In particular, we find that

$$U + iV \sim \frac{3w}{8M} [\mathcal{U}(1-z) - \mathcal{U}(1+z)], \quad (16)$$

as $w \rightarrow \infty$, where

$$\mathcal{U}(Z/w) = \kappa/(1+Z) + 1/(1+\bar{Z}) + (Z+\bar{Z})/(1+\bar{Z})^2, \quad (17)$$

corresponds to a deformation that is only apparent local to the left and right poles, *i.e.* when $z \pm 1 = \mathcal{O}(1/w)$. As the anchoring strength decreases, stress is no longer concentrated at the poles and the maximum shear stress $\tau(x, y) = \sqrt{(\Sigma_{xx} - \Sigma_{yy})^2/4 + \Sigma_{xy}^2}$ (a common indicator of mechanical failure [73]) is greatest at $(\pm x_{\max}, 0)$, where x_{\max} decreases from 1 for $w = \infty$, to 0 for $w \leq 24/35$, see Fig. 2.

For active LCs ($A \neq 0$), the activity leads to an additional deformation:

$$U + iV = U^e + iV^e + A\text{Er}[(1 - \kappa)\rho^2 z + 2\bar{z}]/(4M), \quad (18)$$

where (U^e, V^e) is the deformation of a cylinder immersed in a passive LC. As this addition is proportional to the

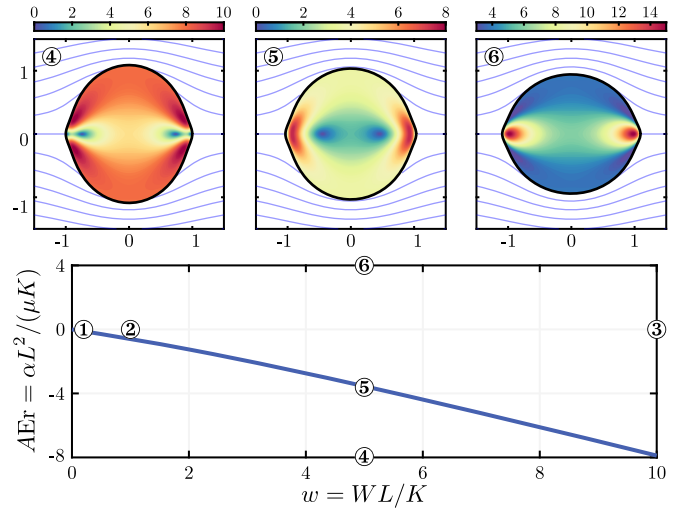


FIG. 3. (top) Deformation of soft cylinders immersed in active nematic LCs with $w = 5$, $M = 50$, $\kappa = 5/3$, and ④ $A\text{Er} = -8 < \mathcal{W}$, ⑤ $A\text{Er} = \mathcal{W} \approx -3.55$, and ⑥ $A\text{Er} = 4 > \mathcal{W}$. Color indicates the maximal shear stress, $\sqrt{(\Sigma_{xx} - \Sigma_{yy})^2/4 + \Sigma_{xy}^2}$, within the cylinder and the blue curves are director lines. (bottom) The critical active Ericksen number, $A\text{Er} = \mathcal{W}$, at which the deformed cylinder has aspect ratio one, plotted as a function of w for $\kappa = 5/3$. The points ①–③ correspond to the configurations shown in Fig. 2.

activity strength, A , activity can act with or against the elastic effects of the LC, depending on if it is extensile ($A < 0$) or contractile ($A > 0$). In particular, the aspect ratio, \mathcal{A}_R , of the deformed cylinder is given by

$$\mathcal{A}_R \sim 1 + U|_{z=1} - V|_{z=i} = 1 + (A\text{Er} - \mathcal{W})/M, \quad (19)$$

where

$$\mathcal{W} = \frac{3\kappa}{2\rho} (\text{arctanh } \rho - \text{arctan } \rho) - \frac{3w}{8}(1 + \kappa). \quad (20)$$

Thus, if $A\text{Er} > \mathcal{W}$ (which includes passive LCs since $\mathcal{W} < 0$), the deformed shape is elongated with the x -axis (*i.e.* the preferred axis of the LC). While, if $A\text{Er} < \mathcal{W}$, the shape is elongated with the y -axis (*i.e.* perpendicular to the preferred axis). The aspect ratio is one at the critical value $A\text{Er} = \mathcal{W}$, see Fig. 3. Therefore, contractile activity ($A > 0$), in this setting, always leads to parallel elongation, while extensile activity ($A < 0$) yields perpendicular elongation, as long as the activity is sufficiently strong.

The fluid flow triggered by the presence of a boundary may also be advantageous in biological cells, settings in which a disperse distribution of molecules, such as nutrients, chemicals, or oxygen, benefit the system's function [75–77]. Consider an active nematic LC bounded inside, and tangentially anchored to, a cylinder with anchoring strength w . Here, the director angle of the LC can be written as

$$\theta = \arg(1 - \rho^2 z^2), \quad (21)$$

for the effective radius introduced in the external problem, $\rho(w) := (\sqrt{1 + 4/w^2} - 2/w)^{1/2}$, while the activity-induced flow can be expressed in terms of a streamfunction

$$\psi = \frac{A}{8} (|z|^2 - 1) \operatorname{Im} \left[\frac{1 - \rho z}{z^2} \log(1 - \rho z) + \frac{1 + \rho z}{z^2} \log(1 + \rho z) \right], \quad (22)$$

see [66]. As before, the elasticity, activity, and viscosity of the LC will induce surface stresses on the boundary, which, if compliant, will deform. Figure 4(a) shows the director lines inside a cylinder that has deformed according to linear elasticity [66]. The final deformed shape resembles a tactoid [78], with a localized deformation at the left and right poles occurring for large anchoring strengths due to the appearance of two +1 aster defects when $w = \infty$. The deformed shape is dependent on the active Ericksen number, $A\text{Er}$, with extensile activity ($A < 0$) leading to parallel elongation and sufficient contractile activity ($A < 0$) yielding perpendicular elongation [66], which is opposite to the aspect ratio's dependence on the activity strength in the external problem.

Figures 4(c-e) show snapshots of the fluid stirring induced by extensile activity. Varying the activity and anchoring strengths primarily affects the speed of stirring, though contractile activity also reverses its direction. The maximum fluid speed, $|\mathbf{u}|_{\max} = \max_{\mathbf{x}} \sqrt{u^2 + v^2}$, is plotted as function of the anchoring strength in Fig. 4(b), for both the LC external and internal to a cylinder. The speeds plateau for large anchoring strengths, $w \gtrsim 10$, and decrease according to $|\mathbf{u}|_{\max} \sim 2|A|w/(25\sqrt{5})$ and $|\mathbf{u}|_{\max} \sim |A|w^2/(600\sqrt{5})$ as $w \rightarrow 0$, for the external and internal problem, respectively. The extent to which this stirring flow results in mixing is an interesting but separate question [79]. Mixing is notoriously challenging in highly viscous flows and in confined geometries [80], but is likely promoted by a wide spatial distribution of active stress [35, 36].

Conclusion: We have shown that the configurations and dynamics of an active nematic can be affected dramatically by the mere presence of an immersed body, or boundary, for any non-trivial anchoring strength. The spontaneous flow that arises is characterized by plumes whose structure is anchoring strength dependent. The elastic, viscous, and active stresses may then deform the body, or external boundary, in a generally localized manner near (virtual) topological defects. Such flows can also produce a spontaneous stirring, and likely mixing, of the environment.

In the above theory, the deformation of the solid was assumed to be small enough that it does not affect the director field. In general, changes in the LC–solid interface could cause the director field to relax towards a different energy-minimizing configuration. Furthermore, although the flow does not directly influence the direc-

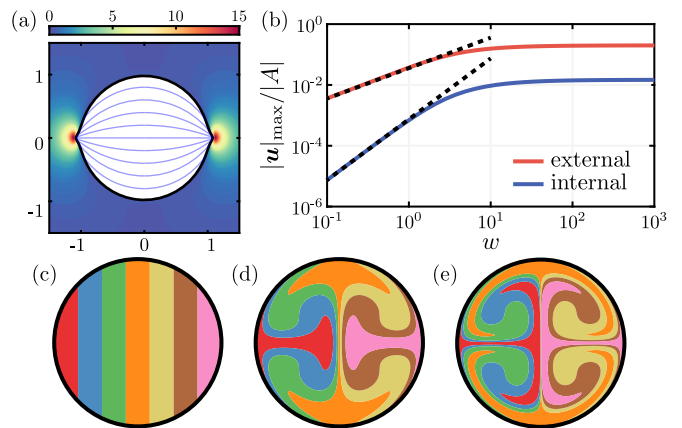


FIG. 4. (a) Deformation of a soft cylinder enclosing a passive nematic LC with $A\text{Er} = 0$, $w = 10$, $M = 50$, and $\kappa = 5/3$. Color delineates the maximum shear stress, $\sqrt{(\Sigma_{xx} - \Sigma_{yy})^2/4 + \Sigma_{xy}^2}$, within the solid and the blue curves are director lines. (b) Plot of the maximum fluid speed, $|\mathbf{u}|_{\max} = \max_{\mathbf{x}} \sqrt{u^2 + v^2}$, as a function of w for the LC external and internal to a cylinder. The asymptotic behaviour as $w \rightarrow 0$, i.e. $|\mathbf{u}|_{\max} \sim 2|A|w/(25\sqrt{5})$ (external) and $|\mathbf{u}|_{\max} \sim |A|w^2/(600\sqrt{5})$ (internal), are shown as black dashed lines. (c-e) Snapshots at times (c) $t = 0$, (d) $t = 100/|A|$, and (e) $t = 200/|A|$ of colored fluid particles transported due to extensile activity inside the cylinder for $w = 10$.

tor field here, boundary deformations do depend on fluid flow, and so, this could provide an indirect influence if the interface deformation was taken into account: flows deform soft boundaries, thereby altering the LC. Even for a simple cylindrical domain, the deformation qualitatively depends on the activity strength (Fig. 3). Thus, since elongated colloids are known to reorient with the preferred axis of the surrounding LC and virtual defects seek out the corners of immersed bodies [70], significant changes to the LC could be expected here. The above work provides the first steps in modelling these complex fluid-structure interactions.

The localized deformations observed have also been reported in tactoids [78] and giant unilamellar vesicles [81]. Even for stiff bodies, the developed points could cause pinning of topological defects, which is important in setting the attraction angle of flexible colloid chains [82], for instance. Additionally, these deformations can encourage surface localized bundling of actin filaments [83, 84].

Looking to the horizon, biological cells are host to a multitude of active anisotropic networks. Can such fluids be triggered into motion solely by the passive anchoring conditions on an arriving organelle? This mechanism could offer an energy-efficient way to generate precisely timed mixing flows within the cellular environment.

Support for this research was provided by the Office of the Vice Chancellor for Research and Graduate Education with funding from the Wisconsin Alumni Research Foundation.

- * tgchandler@wisc.edu
† spagnolie@wisc.edu
- [1] P. Isermann and J. Lammerding, Nuclear mechanics and mechanotransduction in health and disease, *Curr. Biol.* **23**, R1113 (2013).
 - [2] K. Haase, J. K. Macadangang, C. H. Edrington, C. M. Cuerrier, S. Hadjiantoniou, J. L. Harden, I. S. Skerjanc, and A. E. Pelling, Extracellular forces cause the nucleus to deform in a highly controlled anisotropic manner, *Sci. Rep.* **6**, 21300 (2016).
 - [3] R. Ungricht and U. Kutay, Mechanisms and functions of nuclear envelope remodelling, *Nat. Rev. Mol. Cell Biol.* **18**, 229 (2017).
 - [4] F.-Y. Chu, S. C. Haley, and A. Zidovska, On the origin of shape fluctuations of the cell nucleus, *Proc. Natl. Acad. Sci.* **114**, 10338 (2017).
 - [5] E. A. Rog-Zielinska, E. T. O'Toole, A. Hoenger, and P. Kohl, Mitochondrial deformation during the cardiac mechanical cycle, *Anat. Rec.* **302**, 146 (2019).
 - [6] Y. Kalukula, A. D. Stephens, J. Lammerding, and S. Gabriele, Mechanics and functional consequences of nuclear deformations, *Nat. Rev. Mol. Cell Biol.* **23**, 583 (2022).
 - [7] J. C. Del Alamo, G. N. Norwich, Y.-S. J. Li, J. C. Lasheras, and S. Chien, Anisotropic rheology and directional mechanotransduction in vascular endothelial cells, *Proc. Natl. Acad. Sci.* **105**, 15411 (2008).
 - [8] S. K. Gupta, Y. Li, and M. Guo, Anisotropic mechanics and dynamics of a living mammalian cytoplasm, *Soft Matter* **15**, 190 (2019).
 - [9] A. Mogilner and A. Manhart, Intracellular fluid mechanics: Coupling cytoplasmic flow with active cytoskeletal gel, *Annu. Rev. Fluid Mech.* **50**, 347 (2018).
 - [10] N. M. Ramdas and G. Shivashankar, Cytoskeletal control of nuclear morphology and chromatin organization, *J. Mol. Biol.* **427**, 695 (2015).
 - [11] D. Saintillan, M. J. Shelley, and A. Zidovska, Extensile motor activity drives coherent motions in a model of interphase chromatin, *Proc. Natl. Acad. Sci.* **115**, 11442 (2018).
 - [12] M. J. Shelley, The dynamics of microtubule/motor-protein assemblies in biology and physics, *Annu. Rev. Fluid Mech.* **48**, 487 (2016).
 - [13] D. Oriola, D. J. Needleman, and J. Brugués, The physics of the metaphase spindle, *Annu. Rev. Biophys.* **47**, 655 (2018).
 - [14] D. Oriola, F. Jülicher, and J. Brugués, Active forces shape the metaphase spindle through a mechanical instability, *Proc. Natl. Acad. Sci.* **117**, 16154 (2020).
 - [15] I. I. Smalyukh, J. Butler, J. D. ShROUT, M. R. Parsek, and G. C. Wong, Elasticity-mediated nematiclike bacterial organization in model extracellular DNA matrix, *Phys. Rev. E* **78**, 030701 (2008).
 - [16] H.-C. Flemming and J. Wingender, The biofilm matrix, *Nat. Rev. Microbiol.* **8**, 623 (2010).
 - [17] A. Sokolov and I. S. Aranson, Physical properties of collective motion in suspensions of bacteria, *Phys. Rev. Lett.* **109**, 248109 (2012).
 - [18] D. Saintillan, Rheology of active fluids, *Annu. Rev. Fluid Mech.* **50**, 563 (2018).
 - [19] F. Ndlec, T. Surrey, A. C. Maggs, and S. Leibler, Self-organization of microtubules and motors, *Nature* **389**, 305 (1997).
 - [20] C. Dombrowski, L. Cisneros, S. Chatkaew, R. E. Goldstein, and J. O. Kessler, Self-concentration and large-scale coherence in bacterial dynamics, *Phys. Rev. Lett.* **93**, 098103 (2004).
 - [21] D. Saintillan and M. J. Shelley, Instabilities and pattern formation in active particle suspensions: kinetic theory and continuum simulations, *Phys. Rev. Lett.* **100**, 178103 (2008).
 - [22] T. Sanchez, D. T. Chen, S. J. DeCamp, M. Heymann, and Z. Dogic, Spontaneous motion in hierarchically assembled active matter, *Nature* **491**, 431 (2012).
 - [23] A. Doostmohammadi, J. Ignés-Mullol, J. M. Yeomans, and F. Sagués, Active nematics, *Nat. Commun.* **9**, 1 (2018).
 - [24] R. A. Simha and S. Ramaswamy, Hydrodynamic fluctuations and instabilities in ordered suspensions of self-propelled particles, *Phys. Rev. Lett.* **89**, 058101 (2002).
 - [25] G. Subramanian and D. L. Koch, Critical bacterial concentration for the onset of collective swimming, *J. Fluid Mech.* **632**, 359 (2009).
 - [26] S. Ramaswamy, The mechanics and statistics of active matter, *Annu. Rev. Condens. Matter Phys.* **1**, 323 (2010).
 - [27] C. Hohenegger and M. J. Shelley, Stability of active suspensions, *Phys. Rev. E* **81**, 046311 (2010).
 - [28] L. Giomi, L. Mahadevan, B. Chakraborty, and M. Hagan, Banding, excitability and chaos in active nematic suspensions, *Nonlinearity* **25**, 2245 (2012).
 - [29] S. P. Thampi, R. Golestanian, and J. M. Yeomans, Instabilities and topological defects in active nematics, *Europhys. Lett.* **105**, 18001 (2014).
 - [30] S. Weady, Variational bounds and nonlinear stability of an active nematic suspension, *J. Fluid Mech.* **988**, A5 (2024).
 - [31] L. Giomi, Geometry and topology of turbulence in active nematics, *Phys. Rev. X* **5**, 031003 (2015).
 - [32] L. Giomi, L. Mahadevan, B. Chakraborty, and M. F. Hagan, Excitable patterns in active nematics, *Phys. Rev. Lett.* **106**, 218101 (2011).
 - [33] J. Dunkel, S. Heidenreich, K. Drescher, H. H. Wensink, M. Bär, and R. E. Goldstein, Fluid dynamics of bacterial turbulence, *Phys. Rev. Lett.* **110**, 228102 (2013).
 - [34] L. Ohm and M. J. Shelley, Weakly nonlinear analysis of pattern formation in active suspensions, *J. Fluid Mech.* **942**, A53 (2022).
 - [35] A. J. Tan, E. Roberts, S. A. Smith, U. A. Olvera, J. Arteaga, S. Fortini, K. A. Mitchell, and L. S. Hirst, Topological chaos in active nematics, *Nat. Phys.* **15**, 1033 (2019).
 - [36] F. L. Memarian, D. Hammar, M. M. H. Sabbir, M. Elias, K. A. Mitchell, and L. S. Hirst, Controlling chaos: Periodic defect braiding in active nematics confined to a cardioid, *Phys. Rev. Lett.* **132**, 228301 (2024).
 - [37] M. Theillard, R. Alonso-Matilla, and D. Saintillan, Geometric control of active collective motion, *Soft Matter* **13**, 363 (2017).
 - [38] C. Joshi, Z. Zarei, M. M. Norton, S. Fraden, A. Baskaran, and M. F. Hagan, From disks to channels: dynamics of active nematics confined to an annulus, *Soft matter* **19**, 5630 (2023).
 - [39] F. C. Keber, E. Loiseau, T. Sanchez, S. J. DeCamp, L. Giomi, M. J. Bowick, M. C. Marchetti, Z. Dogic, and A. R. Bausch, Topology and dynamics of active nematic

- vesicles, *Science* **345**, 1135 (2014).
- [40] J. Brugués and D. Needleman, Physical basis of spindle self-organization, *Proc. Natl. Acad. Sci.* **111**, 18496 (2014).
- [41] R. Zhang, Y. Zhou, M. Rahimi, and J. J. De Pablo, Dynamic structure of active nematic shells, *Nat. Commun.* **7**, 13483 (2016).
- [42] M. Leoni, O. V. Manyuhina, M. J. Bowick, and M. C. Marchetti, Defect driven shapes in nematic droplets: analogies with cell division, *Soft Matter* **13**, 1257 (2017).
- [43] H. Soni, W. Luo, R. A. Pelcovits, and T. R. Powers, Stability of the interface of an isotropic active fluid, *Soft Matter* **15**, 6318 (2019).
- [44] R. Alert, Fingering instability of active nematic droplets, *J. Phys. A* **55**, 234009 (2022).
- [45] G. Livne, S. Gat, S. Armon, and A. Bernheim-Groswasser, Self-assembled active actomyosin gels spontaneously curve and wrinkle similar to biological cells and tissues, *Proc. Natl. Acad. Sci.* **121**, e2309125121 (2024).
- [46] M. Firouznia and D. Saintillan, Self-organized dynamics of a viscous drop with interfacial nematic activity, arXiv preprint arXiv:2404.11729 (2024).
- [47] A. Mogilner and G. Oster, Cell motility driven by actin polymerization, *Biophys. J.* **71**, 3030 (1996).
- [48] T. Svitkina, The actin cytoskeleton and actin-based motility, *Cold Spring Harbor perspectives in biology* **10**, a018267 (2018).
- [49] C. C. Maass, C. Krüger, S. Herminghaus, and C. Bahr, Swimming droplets, *Annu. Rev. Condens. Matter Phys.* **7**, 171 (2016).
- [50] T. Gao and Z. Li, Self-driven droplet powered by active nematics, *Phys. Rev. Lett.* **119**, 108002 (2017).
- [51] X. Wang, R. Zhang, A. Mozaffari, J. J. de Pablo, and N. L. Abbott, Active motion of multiphase oil droplets: emergent dynamics of squirmers with evolving internal structure, *Soft Matter* **17**, 2985 (2021).
- [52] Y.-N. Young, M. Shelley, and D. Stein, The many behaviors of deformable active droplets, *Math. Biosci. and Eng.* **18** (2021).
- [53] H. Stark, Physics of colloidal dispersions in nematic liquid crystals, *Phys. Rep.* **351**, 387 (2001).
- [54] I. Musevic, *Liquid Crystal Colloids* (Springer, 2017).
- [55] I. I. Smalyukh, Liquid crystal colloids, *Annu. Rev. Condens. Mat. Phys.* **9**, 207 (2018).
- [56] K. Nayani, A. A. Evans, S. E. Spagnolie, and N. L. Abbott, Dynamic and reversible shape response of red blood cells in synthetic liquid crystals, *Proc. Natl. Acad. Sci.* **117**, 26083 (2020).
- [57] R. Zhang, Y. Zhou, J. A. Martínez-González, J. P. Hernández-Ortiz, N. L. Abbott, and J. J. de Pablo, Controlled deformation of vesicles by flexible structured media, *Science Adv.* **2** (2016).
- [58] S. Ray, J. Zhang, and Z. Dogic, Rectified rotational dynamics of mobile inclusions in two-dimensional active nematics, *Phys. Rev. Lett.* **130**, 238301 (2023).
- [59] A. J. H. Houston and G. P. Alexander, Colloids in two-dimensional active nematics: conformational cogs and controllable spontaneous rotation, *New J. Phys.* **25**, 123006 (2023).
- [60] J. B. Freund, Object transport by a confined active suspension, *J. Fluid Mech.* **960**, A16 (2023).
- [61] L. D. Landau, E. M. Lifshitz, A. M. Kosevich, and L. P. Pitaevskii, *Theory of Elasticity*, Vol. 7 (Elsevier, 1986).
- [62] P.-G. De Gennes and J. Prost, *The Physics of Liquid Crystals* (Oxford University Press, 1993).
- [63] I. W. Stewart, *The Static and Dynamic Continuum Theory of Liquid Crystals: A Mathematical Introduction* (Crc Press, 2004).
- [64] M. C. Marchetti, J. F. Joanny, S. Ramaswamy, T. B. Liverpool, J. Prost, M. Rao, and R. A. Simha, Hydrodynamics of soft active matter, *Rev. Mod. Phys.* **85**, 1143 (2013).
- [65] D. Saintillan and M. J. Shelley, Theory of active suspensions, in *Complex Fluids in Biological Systems* (Springer, 2015) pp. 319–351.
- [66] See Supplemental Material at [URL-will-be-inserted-by-publisher] for further mathematical details.
- [67] A. Rapini and M. Papoular, Distorsion d'une lamelle nématique sous champ magnétique conditions d'ancrage aux parois, *J. Phys. Colloq.* **30**, C4 (1969).
- [68] M. J. Ablowitz, A. S. Fokas, and A. S. Fokas, *Complex Variables: Introduction and Applications* (Cambridge University Press, 2003).
- [69] W. E. Langlois and M. O. Deville, *Slow Viscous Flow* (Springer, 1964).
- [70] T. G. J. Chandler and S. E. Spagnolie, A nematic liquid crystal with an immersed body: equilibrium, stress, and paradox, *J. Fluid Mech.* **967**, A19 (2023).
- [71] T. G. J. Chandler and S. E. Spagnolie, Exact and approximate solutions for elastic interactions in a nematic liquid crystal, *SIAM J. Appl. Math.* (in press, 2024).
- [72] A. H. England, *Complex Variable Methods in Elasticity* (Courier Corporation, 2003).
- [73] P. Howell, G. Kozyreff, and J. Ockendon, *Applied Solid Mechanics*, 43 (Cambridge University Press, 2009).
- [74] G. E. Volovik and O. D. Lavrentovich, Topological dynamics of defects: boojums in nematic drops, *Zh. Eksp. Teor. Fiz.* **85**, 1997 (1983).
- [75] N. Fakhri, A. D. Wessel, C. Willms, M. Pasquali, D. R. Klopfenstein, F. C. MacKintosh, and C. F. Schmidt, High-resolution mapping of intracellular fluctuations using carbon nanotubes, *Science* **344**, 1031 (2014).
- [76] E. F. Koslover, C. K. Chan, and J. A. Theriot, Cytoplasmic flow and mixing due to deformation of motile cells, *Biophys. J.* **113**, 2077 (2017).
- [77] S. S. Mogre, A. I. Brown, and E. F. Koslover, Getting around the cell: physical transport in the intracellular world, *Phys. Biol.* **17**, 061003 (2020).
- [78] C. D. Schimming and J. Viñals, Equilibrium morphology of tactoids in elastically anisotropic nematics, *Soft Matter* **18**, 8024 (2022).
- [79] E. Villermaux, Mixing versus stirring, *Annu. Rev. Fluid Mech.* **51**, 245 (2019).
- [80] E. Guillard, N. Kuncio, O. Dauchot, B. Dubrulle, S. Roux, and J.-L. Thiffeault, Walls inhibit chaotic mixing, *Phys. Rev. Lett.* **99**, 114501 (2007).
- [81] P. C. Mushenheim, J. S. Pendery, D. B. Weibel, S. E. Spagnolie, and N. L. Abbott, Straining soft colloids in aqueous nematic liquid crystals, *Proc. Natl. Acad. Sci.* **113**, 5564 (2016).
- [82] A. DeBenedictis, T. J. Atherton, A. L. Rodarte, and L. S. Hirst, Modeling deformation and chaining of flexible shells in a nematic solvent with finite elements on an adaptive moving mesh, *Phys. Rev. E* **97**, 032701 (2018).
- [83] A. P. Liu, D. L. Richmond, L. Maibaum, S. Pronk, P. L. Geissler, and D. A. Fletcher, Membrane-induced bundling of actin filaments, *Nat. Phys.* **4**, 789 (2008).
- [84] M. S. E. Peterson, A. Baskaran, and M. F. Hagan, Vesicle

cle shape transformations driven by confined active filaments, *Nat. Commun.* **12**, 7247 (2021).

Supplemental material for “Active nematic response to a deformable body or boundary: elastic deformations and anchoring-induced flow”

Thomas G. J. Chandler^{1,*} and Saverio E. Spagnolie^{1,†}

¹*Department of Mathematics, University of Wisconsin–Madison, Madison, WI 53706, USA*

(Dated: September 25, 2024)

GOVERNING EQUATIONS

Recall that, according to Erickson–Leslie theory with the one-constant approximation, the director field \mathbf{n} and fluid velocity \mathbf{u} evolve according to Eqs. (1)–(3) in the main text. Non-dimensionalizing this system using a length scale L , velocity scale U , and time scale L/U yields

$$\partial_t \mathbf{n} + \mathbf{u} \cdot \nabla \mathbf{n} = \mathbf{n} \cdot \boldsymbol{\Omega} + \lambda \mathbf{n} \cdot \mathbf{E} \cdot (\mathbf{I} - \mathbf{n}\mathbf{n}) + \tilde{\mathbf{h}}/\gamma' \text{Er}, \quad (\text{S1a})$$

$$\nabla \cdot (\boldsymbol{\sigma}^e + \text{Er} \boldsymbol{\sigma}^v + A \text{Er} \boldsymbol{\sigma}^a - \text{Er} p \mathbf{I}) = \mathbf{0} \quad \text{and} \quad \nabla \cdot \mathbf{u} = 0, \quad (\text{S1b,c})$$

for the strain rate tensor $\mathbf{E} = (\nabla \mathbf{u} + \nabla \mathbf{u}^T)/2$, vorticity tensor $\boldsymbol{\Omega} = (\nabla \mathbf{u} - \nabla \mathbf{u}^T)/2$, projected molecular field $\tilde{\mathbf{h}} = (\mathbf{I} - \mathbf{n}\mathbf{n}) \cdot \nabla^2 \mathbf{n}$, and elastic, viscous, and active stress tensors

$$\boldsymbol{\sigma}^e = -\nabla \mathbf{n} \cdot \nabla \mathbf{n}^T + \frac{1}{2}(1 - \lambda) \mathbf{n} \tilde{\mathbf{h}} - \frac{1}{2}(1 + \lambda) \tilde{\mathbf{h}} \mathbf{n}, \quad (\text{S2a})$$

$$\boldsymbol{\sigma}^v = 2\mathbf{E} + \mu'_1 (\mathbf{n} \cdot \mathbf{E} \cdot \mathbf{n}) \mathbf{n}\mathbf{n} + \mu'_2 (\mathbf{n}\mathbf{E} \cdot \mathbf{n} + \mathbf{n} \cdot \mathbf{E}\mathbf{n}), \quad (\text{S2b})$$

$$\boldsymbol{\sigma}^a = 2\mathbf{n}\mathbf{n}, \quad (\text{S2c})$$

respectively. Here, A , Er , λ , γ' , μ'_1 , and μ'_2 are the dimensionless parameters defined in the main text and $\mathbf{n}\mathbf{n}$ and similar are dyadic products.

For small viscosity ratios and rotational Erickson number, $\gamma', \mu'_i, \gamma' \text{Er} \ll 1$, the stress tensors reduce to

$$\boldsymbol{\sigma}^e = -\nabla \mathbf{n} \cdot \nabla \mathbf{n}^T + \mathcal{O}(\gamma' \text{Er}), \quad (\text{S3a})$$

$$\boldsymbol{\sigma}^v = \nabla \mathbf{u} + \nabla \mathbf{u}^T + \mathcal{O}(\mu'_i \text{Er}), \quad (\text{S3b})$$

$$\boldsymbol{\sigma}^a = 2\mathbf{n}\mathbf{n}. \quad (\text{S3c})$$

Inserting these into (S1) yields the asymptotic system found in the main text:

$$\tilde{\mathbf{h}} = (\mathbf{I} - \mathbf{n}\mathbf{n}) \cdot \nabla^2 \mathbf{n} = \mathcal{O}(\gamma' \text{Er}), \quad \nabla \cdot \mathbf{u} = 0, \quad (\text{S4a,b})$$

$$\nabla^2 \mathbf{u} - \nabla p = \frac{1}{\text{Er}} \nabla \cdot (\nabla \mathbf{n} \cdot \nabla \mathbf{n}^T) - 2A \nabla \cdot (\mathbf{n}\mathbf{n}) = \mathcal{O}(\gamma', \mu'_i). \quad (\text{S4c})$$

Two-dimensional theory

In 2D, the LC can be described by a director angle, $\theta(x, y)$, and a streamfunction, $\psi(x, y)$, such that $\mathbf{n} = (\cos \theta, \sin \theta)$ and $\mathbf{u} = (\psi_y, -\psi_x)$. Here, we absorb the isotropic parts of the stress tensors, (S3), into the pressure by taking $p \mapsto p + A - |\nabla \theta|^2/(2\text{Er})$. At leading-order, the system (S4) is then

$$\nabla^2 \theta = 0, \quad (\text{S5a})$$

$$\partial_y \omega - \partial_x p = A [\partial_x \cos(2\theta) + \partial_y \sin(2\theta)], \quad (\text{S5b})$$

$$\partial_x \omega + \partial_y p = A [\partial_y \cos(2\theta) - \partial_x \sin(2\theta)], \quad (\text{S5c})$$

with vorticity $\omega = -\nabla^2 \psi$. On any immersed or confining boundaries, the fluid velocity vanishes and the director field is subject to Rapini–Papoular anchoring [S1, S2], *i.e.*

$$\partial_x \psi = \partial_y \psi = 0 \quad \text{and} \quad \partial_\nu \theta = \frac{w}{2} \sin[2(\theta - \phi)], \quad (\text{S6a,b})$$

respectively, where w is the dimensionless anchoring strength (as defined in main text), ϕ is the preferred director orientation on the boundary, and $\partial_\nu = \hat{\boldsymbol{\nu}} \cdot \nabla$ is a normal derivative for the unit normal vector pointing into the LC $\hat{\boldsymbol{\nu}}$.

Here, the traceless stress tensors are denoted with hats:

$$\hat{\boldsymbol{\sigma}}^e = \frac{1}{2}(\partial_y\theta - \partial_x\theta)(\mathbf{x}\mathbf{x} - \mathbf{y}\mathbf{y}) - \partial_x\theta\partial_y\theta(\mathbf{x}\mathbf{y} + \mathbf{y}\mathbf{x}), \quad (\text{S7a})$$

$$\hat{\boldsymbol{\sigma}}^v = 2\partial_{xy}\psi(\mathbf{x}\mathbf{x} - \mathbf{y}\mathbf{y}) + (\partial_{yy}\psi - \partial_{xx}\psi)(\mathbf{x}\mathbf{y} + \mathbf{y}\mathbf{x}), \quad (\text{S7b})$$

$$\hat{\boldsymbol{\sigma}}^a = \cos(2\theta)(\mathbf{x}\mathbf{x} - \mathbf{y}\mathbf{y}) + \sin(2\theta)(\mathbf{x}\mathbf{y} + \mathbf{y}\mathbf{x}), \quad (\text{S7c})$$

where \mathbf{x} and \mathbf{y} are the unit vectors in the x and y directions, respectively. The elastic and activity-induced stresses acting on a surface are

$$\mathbf{t}^e = \hat{\boldsymbol{\nu}} \cdot \hat{\boldsymbol{\sigma}}^e + \partial_s \mathbf{t}^s \quad \text{and} \quad \mathbf{t}^a = \text{Er} \hat{\boldsymbol{\nu}} \cdot (\hat{\boldsymbol{\sigma}}^v + A\hat{\boldsymbol{\sigma}}^a - p\mathbf{I}), \quad (\text{S8a})$$

respectively, for the surface stress vector (which comes from the surface anchoring condition [S2])

$$\mathbf{t}^s = \frac{w}{2} (\sin(\theta - \phi)^2 \hat{\mathbf{s}} + \sin[2(\theta - \phi)] \hat{\boldsymbol{\nu}}), \quad (\text{S9})$$

boundary arclength s (which is oriented such that the LC is on the right), unit tangent vector $\hat{\mathbf{s}} = (x_s, y_s)$, and unit normal vector $\hat{\boldsymbol{\nu}} = (y_s, -x_s)$.

Changing coordinates from x and y to the complex position $z = x + iy$ and its complex conjugate $\bar{z} = x - iy$ yields the system (S5) introduced in the main text. This can be solved analytically to give

$$\theta = -\arg f'(z), \quad p - i\omega = A\partial_z [g(z) + \overline{f(\bar{z})}/f'(z)], \quad \psi = \frac{A}{4} \text{Im} \left[\bar{z}g(z) + h(z) + \overline{\int f(z) dz / f'(z)} \right], \quad (\text{S10a-c})$$

for functions f , g , and h , which are locally holomorphic in the LC and satisfy the boundary conditions (S6). From these we can compute the fluid velocity

$$u - iv = 2i\psi_z = \frac{A}{4} \left[\bar{z}g'(z) - \overline{g(z)} + h'(z) + \partial_z \left(\frac{\overline{\int f(z) dz}}{f'(z)} \right) - \frac{f(z)}{f'(z)} \right]. \quad (\text{S11})$$

On a bounding surface, \bar{z} can be related to z using the boundary's Schwarz function [S3] and the surface tractions can be computed using

$$t_x^e - it_y^e = 2i(\partial_z\theta)^2\partial_s z + \partial_s(t_x^s - it_y^s), \quad (\text{S12a})$$

$$t_x^a - it_y^a = \text{Er}([4\partial_{zz}\psi - iAe^{-2i\theta}]\partial_s z - ip\partial_s\bar{z}), \quad (\text{S12b})$$

$$t_x^s - it_y^s = \frac{w}{8} (2 + e^{2i(\theta-\phi)} - 3e^{2i(\phi-\theta)})\partial_s\bar{z}. \quad (\text{S12c})$$

Solid deformation

According to plane stress/strain in linear elastostatics, the deformation, (U, V) , and stress tensor, $\boldsymbol{\Sigma}$, of an isotropic elastic solid can be written in terms of an Airy stress function, $\mathcal{A}(x, y)$, which satisfies the biharmonic equation, $\nabla^4\mathcal{A} = 0$ [S4, S5]. This biharmonic function can be written in terms of two Goursat functions, G and H , that is

$$\mathcal{A} = \text{Im} [\bar{z}G(z) + H(z)], \quad (\text{S13})$$

where G and H are locally holomorphic in the solid and satisfy the stress balance on the LC–solid interface, $-\hat{\boldsymbol{\nu}} \cdot \boldsymbol{\Sigma} = \mathbf{t}^e + \mathbf{t}^a$. The solid stress tensor, $\boldsymbol{\Sigma}$, is given by the Kolosov–Muskhelishvili formulae,

$$\Sigma_{xx} - \Sigma_{yy} - 2i\Sigma_{xy} = 2i\bar{z}G''(z) + 2iH''(z) \quad \text{and} \quad \Sigma_{xx} + \Sigma_{yy} = 4 \text{Im} G'(z), \quad (\text{S14a,b})$$

where subscripts denote tensor elements, and the solid displacement, (U, V) , is given by

$$2M(U - iV) = i\kappa\overline{G(z)} + i\bar{z}G'(z) + iH'(z). \quad (\text{S15})$$

where M and κ are the dimensionless elastic modulus and Muskhelishvili constant defined in the main text. Using (S12) and (S14), the first integral of the interface stress balance is

$$\bar{z}G'(z) - \overline{G(z)} + H'(z) = \int t_x^e - it_y^e + t_x^a - it_y^a ds, \quad (\text{S16})$$

where \bar{z} is related to z using the Schwarz function for the interface. This stress balance is unique up to an arbitrary integration constant.

EXAMPLE 1: CYLINDER IMMERSED IN AN ACTIVE LC

In this section, we derive analytical expressions for the director field, streamfunction, and Airy stress function associated with the first example considered in the main text: a soft unit cylinder immersed in a weakly-active nematic LC, subject to (finite) tangential anchoring.

Director field

Chandler and Spagnolie [S2] showed that the director field can be expressed in terms of a potential function $f(z)$ such that $\theta = -\arg f'$. Here, $f(z)$ must be holomorphic in $\rho < |z| < \infty$, have a constant imaginary-part on $|z| = \rho$, and satisfy $f(z) \sim z$ as $|z| \rightarrow \infty$, for the effective/virtual radius $\rho(w) = (\sqrt{1 + 4/w^2} - 2/w)^{1/2}$. By Milne-Thomson circle theorem, this has solution

$$f(z) = z + \rho^2/z. \quad (\text{S17})$$

(Note that this is unique up to an additive imaginary logarithm, $i\gamma \log z$ for $\gamma \in \mathbb{R}$. We shall only consider the case when $\gamma = 0$ as this corresponds to the up-down symmetric case, which minimizes the (Frank) elastic energy [S2].) This potential yields the director angle given in the main text,

$$\theta = -\arg f'(z) = -\arg(1 - \rho^2/z^2), \quad (\text{S18})$$

which holds for all anchoring strengths $w > 0$.

Streamfunction

Inserting (S17) into (S10c) yields the streamfunction

$$\psi = \frac{A}{4} \text{Im} \left[\bar{z}g(z) + h(z) + \frac{\bar{z}^2/2 + \rho^2 \log \bar{z}}{1 - \rho^2/z^2} \right], \quad (\text{S19})$$

for the two Goursat functions $h(z)$ and $g(z)$, which are locally holomorphic in $1 < |z| < \infty$ and yield a fluid velocity that vanishes on $|z| = 1$ and as $|z| \rightarrow \infty$.

Firstly, to ensure ψ is single-valued around $|z| = 1$, let $h(z) = \tilde{h}(z) + \rho^2 \log z/(1 - \rho^2/z^2)$:

$$\psi = \frac{A}{4} \text{Im} \left[\bar{z}g(z) + \tilde{h}(z) + \frac{\bar{z}^2/2 + 2\rho^2 \log |z|}{1 - \rho^2/z^2} \right]. \quad (\text{S20})$$

We now need to find g and \tilde{h} such that the fluid velocity,

$$u - iv = 2i\partial_z \psi = \frac{A}{4} \left[\bar{z}g'(z) + \tilde{h}'(z) - \bar{g}(\bar{z}) - \frac{z + \rho^2/z}{1 - \rho^2/\bar{z}^2} - \frac{2\rho^2 (\bar{z}^2 - z^2)/2 + \rho^2/2 + 2\rho^2 \log |z|}{z^3 (1 - \rho^2/z^2)^2} \right], \quad (\text{S21})$$

vanishes on $|z| = 1$ and as $|z| \rightarrow \infty$. Note that the pressure and vorticity are given by (S10b), which is

$$p - i\omega = A \left(g'(z) + \partial_z \frac{\bar{z} + \rho^2/\bar{z}}{1 - \rho^2/z^2} \right). \quad (\text{S22})$$

Consider the functions

$$g(z) = \mathcal{G}(z) - \frac{\rho^2(1 + \rho^2 z^2)}{z(z^2 - \rho^2)} \quad \text{and} \quad \tilde{h}(z) = \mathcal{H}(z) + \frac{z^2}{2} - \frac{1}{2z^2} + \frac{1/2 + \rho^4}{z^2 - \rho^2}. \quad (\text{S23a,b})$$

These are holomorphic in $1 < |z| < \infty$ provided \mathcal{G} and \mathcal{H} are holomorphic there. Furthermore,

$$u - iv = \frac{A}{4} [(1/z)\mathcal{G}'(z) + \mathcal{H}'(z) - \bar{\mathcal{G}}(1/\bar{z})] \quad \text{on } |z| = 1, \quad (\text{S24a})$$

$$\text{and } u - iv \sim \frac{A}{4} [\bar{z}\mathcal{G}'(z) + \mathcal{H}'(z) - \bar{\mathcal{G}}(\bar{z})] \quad \text{as } |z| \rightarrow \infty, \quad (\text{S24b})$$

which both vanish provided $\mathcal{H}'(z) = \bar{\mathcal{G}}(1/z) - \mathcal{G}'(z)/z$, $\mathcal{G}(z) \sim az + b$ as $|z| \rightarrow \infty$, and $\mathcal{H}'(z) \sim \bar{b}$ as $|z| \rightarrow \infty$, for $a \in \mathbb{R}$ and $b \in \mathbb{C}$. Since \mathcal{G} and \mathcal{H} are holomorphic in $1 < |z| < \infty$, they can be expressed as Laurent expansions around $z = 0$. It immediately follows that $\mathcal{G}(z) = az + b$ and $\mathcal{H}(z) = \bar{b}z + c$ for $c \in \mathbb{C}$. Here, b and c are complex constants that can be set to zero, without loss of generality, while a is a real constant that sets the reference pressure at infinity,

$$p - i\omega \sim Aa \text{ as } |z| \rightarrow \infty, \quad (\text{S25})$$

which we also take to be zero.

Inserting (S23) into (S20) and (S21) with $\mathcal{G} = \mathcal{H} = 0$ yields the streamfunction given in the main text,

$$\psi = \frac{A\rho^2}{8} \text{Im} \left[\frac{(|z|^2 - 1)^2}{z^2(z^2 - \rho^2)} + \frac{1 - |z|^2 + 2 \log |z|}{(z^2 - \rho^2)/(2\rho^2)} \right], \quad (\text{S26})$$

and the fluid velocity

$$u - iv = 2i\partial_z\psi = \frac{A\rho^2}{4}(|z|^2 - 1) \left[\frac{2/z - \bar{z} + \rho^2(z - 1/z^3) + \rho^4/z}{(z^2 - \rho^2)^2} - \frac{1/\bar{z} - \rho^2/z}{\bar{z} - \rho^2} \right] - \frac{A\rho^4 z \log |z|}{(z^2 - \rho^2)^2}. \quad (\text{S27})$$

Furthermore, using $z_s = iz$, $\bar{z} = 1/z$, and $w = 4\rho^2/(1 - \rho^4)$, the tractions (S12) acting on $|z| = 1$ are

$$t_x^e - it_y^e = \frac{3z(1/\rho^2 + z^2)}{2(1/\rho^2 - z^2)^2} - \frac{3z(z^2 - 3\rho^2)}{2(z^2 - \rho^2)^2} + \frac{3 + \rho^2}{1 + \rho^2} \frac{1}{2z} \quad \text{and} \quad t_x^a - it_y^a = A\text{Er} \left(z - \frac{\rho^2}{z} \right). \quad (\text{S28a,b})$$

Airy stress function

We next find the solid Goursat functions $G(z)$ and $H(z)$, which must be holomorphic in $|z| < 1$ and satisfy the stress balance (S16) on $|z| = 1$. Integrating the surface tractions given in (S28), and imposing $\bar{z} = 1/z$ and $z_s = iz$, we find that the stress balance can be expressed as

$$\frac{1}{z}G'(z) - \bar{G}(1/z) + H'(z) = \frac{i(3 + \rho^2)}{2z(1 + \rho^2)} + \frac{3iz/2}{z^2 - \rho^2} + \frac{3iz/2}{z^2 - 1/\rho^2} + \frac{3i}{2\rho} \log \frac{1 - \rho/z}{1 + \rho/z} - iA\text{Er} \left(z + \frac{\rho^2}{z} \right). \quad (\text{S29})$$

The trick to finding G and H here is to use that $G(z)$ and $H'(z)$ are holomorphic in $|z| < 1$, while $\bar{G}(1/z)$ is holomorphic in $|z| > 1$; this allows one to match the terms on the left-hand side of (S29) with those on the right-hand side.

Consider the functions

$$G(z) = \mathcal{G}(z) + \frac{3 + 2\rho^2}{1 + \rho^2} \frac{iz}{2} + \frac{3iz/(2\rho^2)}{1/\rho^2 - z^2} - \frac{3i}{2\rho} \log \frac{1/\rho + z}{1/\rho - z} - iA\text{Er} \frac{\rho^2 z}{2}, \quad (\text{S30a})$$

$$\text{and } H(z) = \mathcal{H}(z) - \frac{3iz^2/2}{1/\rho^2 - z^2} - iA\text{Er} \frac{z^2}{2}, \quad (\text{S30b})$$

These are holomorphic in $|z| < 1$ as long as \mathcal{G} and \mathcal{H} are holomorphic there, and (S29) is satisfied provided $\mathcal{H}'(z) = \bar{\mathcal{G}}(1/z) - \mathcal{G}'(z)/z$. As \mathcal{G} and \mathcal{H} are holomorphic at $z = 0$, they can be expressed as Taylor expansions around $z = 0$. It follows that $\mathcal{G}(z) = az + b$ and $\mathcal{H}(z) = \bar{b}z + c$ for $a \in \mathbb{R}$ and $b, c \in \mathbb{C}$. Constant c is arbitrary and can be set to zero, while b and a correspond to a rigid body motion. In particular, using the displacement equation (S15) with (S30), the origin is rotated anticlockwise by the signed angle $-a(1 + \kappa)/(2M)$ and is displaced by $U_0 + iV_0 = i\bar{b}(1 + \kappa)/(2M)$. We set a and b to zero so that the origin and its orientation are preserved.

Overall, inserting (S30) with $\mathcal{G} = \mathcal{H} = 0$ into (S14) and (S15) gives the stress and displacement of the cylinder, respectively. The deformed cylinder's aspect ratio and the asymptotic displacement as $w \rightarrow \infty$ given in the main text follow from these expressions.

EXAMPLE 2: CYLINDER CONFINING AN ACTIVE LC

In this section, we derive analytical expressions for the director field, streamfunction, and Airy stress function associated with the second example considered in the main text: a weakly-active nematic LC inside a soft unit cylinder, subject to (finite) tangential anchoring.

Director field

Using the effective/virtual boundary technique presented in Ref. [S2], the director angle can be described by a potential function $f(z)$, which is holomorphic in $|z| < 1/\rho$ and has a constant imaginary-part on $|z| = 1/\rho$, where $\rho(w) = (\sqrt{1 + 4/w^2} - 2/w)^{1/2}$. This problem has the solution

$$f(z) = \frac{1}{2\rho} \log(1 + \rho z) - \frac{1}{2\rho} \log(1 - \rho z), \quad (\text{S31})$$

yielding the director angle

$$\theta(z) = -\arg f'(z) = \arg(1 - \rho^2 z^2). \quad (\text{S32})$$

This solution hold for all anchoring strengths $w > 0$.

Streamfunction

Inserting the potential (S31) into (S10b) yields the fluid pressure and vorticity,

$$p - i\omega = A \left(g'(z) - \rho z \log \frac{1 + \rho \bar{z}}{1 - \rho \bar{z}} \right), \quad (\text{S33})$$

while (S10c) yields the streamfunction

$$\psi = \frac{A}{4} \text{Im} \left[h(z) + \bar{z}g(z) - \frac{z^2}{2} \log(1 - \rho^2 \bar{z}^2) - \rho \frac{\bar{z}z^2}{2} \log \frac{1 + \rho \bar{z}}{1 - \rho \bar{z}} \right]. \quad (\text{S34})$$

The fluid velocity can then be computed by taking a partial derivative of ψ with respect to z , that is

$$u - iv = 2i\partial_z \psi = \frac{A}{4} \left[h'(z) + \bar{z}g'(z) - \bar{g}(\bar{z}) + \frac{\rho \bar{z}^2}{2} \log \frac{1 - \rho z}{1 + \rho z} - \rho \bar{z}z \log \frac{1 + \rho \bar{z}}{1 - \rho \bar{z}} - z \log(1 - \rho^2 z^2) \right]. \quad (\text{S35})$$

Note that these expressions are continuous in $|z| \leq 1$ provided h and g are holomorphic there. We now find the Goursat functions h and g , which yield a fluid velocity, (S35), that vanishes on $|z| = 1$.

Consider the functions

$$g(z) = \mathcal{G}(z) - \frac{1}{z}(1 - \rho z) \log(1 - \rho z) - \frac{1}{z}(1 + \rho z) \log(1 + \rho z) + \rho^2 z, \quad (\text{S36a})$$

$$\text{and } h(z) = \mathcal{H}(z) + \frac{1}{2z^2}(1 - \rho z) \log(1 - \rho z) + \frac{1}{2z^2}(1 + \rho z) \log(1 + \rho z). \quad (\text{S36b})$$

These are holomorphic in $|z| \leq 1$ as long as \mathcal{G} and \mathcal{H} are holomorphic there. Furthermore, they yield

$$u - iv = \frac{A}{4} [\mathcal{G}'(z)/z + \mathcal{H}'(z) - \bar{\mathcal{G}}(1/z)] \text{ on } |z| = 1, \quad (\text{S37})$$

which vanishes provided $\mathcal{H}'(z) = \bar{\mathcal{G}}(1/z) - (1/z)\mathcal{G}'(z)$. As with the previous example, inserting a Taylor expansion for $\mathcal{G}(z)$ and $\mathcal{H}(z)$ around $z = 0$ yields $\mathcal{G}(z) = az + b$ and $\mathcal{H}(z) = \bar{b}z + c$ for $a \in \mathbb{R}$ and $b, c \in \mathbb{C}$. Here, b and c are arbitrary, and so can be set to zero, while a sets the reference pressure at the origin,

$$p - i\omega \sim Aa \text{ as } |z| \rightarrow 0. \quad (\text{S38})$$

which we assume to vanish.

Overall, inserting (S36) with $\mathcal{G} = \mathcal{H} = 0$ into (S34) yields the streamfunction given in the main text,

$$\psi = \frac{A}{8} (|z|^2 - 1) \text{Im} \left[\frac{1 - \rho z}{z^2} \log(1 - \rho z) + \frac{1 + \rho z}{z^2} \log(1 + \rho z) \right], \quad (\text{S39})$$

while the fluid pressure, vorticity, and velocity follow from (S33) and (S35). Furthermore, using $z_s = -iz$, $\bar{z} = 1/z$, and $w = 4\rho^2/(1 - \rho^4)$, the tractions (S12) acting on $|z| = 1$ are given by

$$t_x^e - it_y^e = \frac{\rho^2 z(3 - \rho^2 z^2)}{2(1 - \rho^2 z^2)^2} + \frac{z(z^2 + \rho^2)}{2(z^2 - \rho^2)^2} - \frac{1 + 3\rho^2}{1 + \rho^2} \frac{1}{2z}, \quad (\text{S40a})$$

$$\text{and } t_x^a - it_y^a = A \text{Er} \left[z \log(1 - \rho^2/z^2) + \frac{\rho}{z^2} \log \frac{1 - \rho z}{1 + \rho z} - \frac{1 - \rho^4}{1/z - \rho^2 z} + \frac{2\rho^2}{z} \right]. \quad (\text{S40b})$$

Airy stress function

The solid Goursat functions, $G(z)$ and $H(z)$, must be locally holomorphic in $1 < |z| < \infty$, yield a displacement that vanishes as $|z| \rightarrow \infty$, and satisfy the stress balance (S16) on $|z| = 1$. Integrating the surface tractions (S40) and using $\bar{z} = 1/z$ and $z_s = -iz$, we find that the stress balance can be expressed as

$$\frac{1}{z}G'(z) - \bar{G}(1/z) + H'(z) = \int t_x^e - it_y^e ds + \int t_x^a - it_y^a ds, \quad (\text{S41})$$

where

$$\int t_x^e - it_y^e ds = -\frac{\rho i}{2} \log \frac{1 - \rho z}{1 + \rho z} - \frac{iz/2}{z^2 - 1/\rho^2} - \frac{iz/2}{z^2 - \rho^2} + \frac{1 + 3\rho^2}{1 + \rho^2} \frac{i}{2z}, \quad (\text{S42a})$$

$$\text{and } \int t_x^a - it_y^a ds = iA\text{Er} \left[z \log(1 - \rho^2/z^2) + \rho \log \frac{z + \rho}{z - \rho} + \left(\frac{1}{2\rho} - \frac{\rho}{2z^2} \right) \log \frac{1 - \rho z}{1 + \rho z} - \frac{\rho^2}{z} \right]. \quad (\text{S42b})$$

Here, we can equate the $G'(z)$ and $H'(z)$ terms on the left-hand side of (S41) with the terms holomorphic in $|z| > 1$ on the right-hand side. Similarly, the $\bar{G}(1/z)$ term is identified with the terms holomorphic in $|z| < 1$.

Consider the functions

$$G(z) = \mathcal{G}(z) + \frac{i\rho}{2} \log \frac{z + \rho}{z - \rho} + \frac{i\rho^2 z/2}{z^2 - \rho^2} + iA\text{Er} \left[\frac{\rho^2 z^2 - 1}{2\rho} \log \frac{z + \rho}{z - \rho} - \rho^2 z \right], \quad (\text{S43a})$$

$$\text{and } H(z) = \mathcal{H}(z) + \frac{i\rho^2}{1 + \rho^2} \log z - \frac{i\rho^2/2}{z^2 - \rho^2} + iA\text{Er} \left[\frac{z^2 - 1/\rho^2}{2} \log(1 - \rho^2/z^2) + \rho^2 \log z \right]. \quad (\text{S43b})$$

These are locally holomorphic in $1 < |z| < \infty$ provided $\mathcal{G}(z)$ and $\mathcal{H}(z)$ are locally holomorphic there, also (S41) is satisfied provided $\mathcal{H}'(z) = \bar{\mathcal{G}}(1/z) - \mathcal{G}'(z)/z$. Since $G(z) \sim \mathcal{G}(z)$ and $H'(z) \sim \mathcal{H}'(z)$ as $|z| \rightarrow \infty$, the displacement of the solid, (S15), satisfies

$$2M(U - iV) \sim i\kappa \overline{\mathcal{G}(z)} + i\bar{z}\mathcal{G}'(z) + i\mathcal{H}'(z) \text{ as } |z| \rightarrow \infty, \quad (\text{S44})$$

which vanishes only if $\mathcal{G}(z) = 0$ and $\mathcal{H}(z) = c$ for some arbitrary constant $c \in \mathbb{C}$, which we set to zero.

Overall, inserting (S43) with $\mathcal{G} = \mathcal{H} = 0$ into (S14) and (S15) yields the stress and displacement of the solid. For large anchoring strengths, $w \rightarrow \infty$, we find that

$$U + iV \sim \frac{w}{8M} [\mathcal{U}(z - 1) - \mathcal{U}(-1 - z)], \quad (\text{S45})$$

for the localized deformation

$$\mathcal{U}(Z/w) = \kappa/(1 + Z) + 1/(1 + \bar{Z}) + (Z + \bar{Z})/(1 + \bar{Z})^2. \quad (\text{S46})$$

which is only apparent local to the left and right poles, *i.e.* when $z \pm 1 = \mathcal{O}(1/w)$. Note that this closely resembles the asymptotic expression found for the immersed cylinder example, as discussed in the main text. For a general anchoring strength, the aspect ratio of the deformed shape is given by

$$\mathcal{A}_R \sim 1 + U|_{z=1} - V|_{z=i} = 1 + (\mathcal{W}_1 - A\text{Er}\mathcal{W}_2)/M, \quad (\text{S47})$$

with

$$\mathcal{W}_1 = \frac{\kappa\rho}{2} (\text{arctanh } \rho + \arctan \rho) + \frac{w}{8}(1 + \kappa), \quad (\text{S48a})$$

$$\text{and } \mathcal{W}_2 = \frac{\kappa}{2\rho} (\text{arctanh } \rho + \arctan \rho) + \rho(1 - \kappa/2)(\text{arctanh } \rho - \arctan \rho) + \frac{1}{2} \log(1 - \rho^4). \quad (\text{S48b})$$

Since $\mathcal{W}_1, \mathcal{W}_2 \geq 0$, we find that the deformed shape is elongated with the y -axis if $A\text{Er} > \mathcal{W}_1/\mathcal{W}_2$ and elongated with the x -axis if $A\text{Er} < \mathcal{W}_1/\mathcal{W}_2$. Therefore, extensile activity ($A < 0$) always leads to parallel elongation, while contractile activity ($A > 0$) yields perpendicular elongation, as long as the activity is sufficiently strong. Note that this is in direct contrast to immersed cylinder example, which was discussed in the main text.

* tgchandler@wisc.edu

[†] spagnolie@wisc.edu

- [S1] A. Rapini and M. Papoular, Distorsion d'une lamelle nématique sous champ magnétique conditions d'ancrage aux parois, *J. Phys. Colloq.* **30**, C4 (1969).
- [S2] T. G. J. Chandler and S. E. Spagnolie, A nematic liquid crystal with an immersed body: equilibrium, stress, and paradox, *J. Fluid Mech.* **967**, A19 (2023).
- [S3] M. J. Ablowitz, A. S. Fokas, and A. S. Fokas, *Complex Variables: Introduction and Applications* (Cambridge University Press, 2003).
- [S4] A. H. England, *Complex Variable Methods in Elasticity* (Courier Corporation, 2003).
- [S5] P. Howell, G. Kozyreff, and J. Ockendon, *Applied Solid Mechanics*, 43 (Cambridge University Press, 2009).